Modeling of the Impact of Blood Vessel Flow on the Temperature Distribution during Focused Ultrasound Exposure

E. Sassaroli[1], K.C. P. Li[1] and B. E. O'Neill[*,1]
[1]The Methodist Hospital Research Institute, Houston, TX, 77030, USA
*Corresponding author: The Methodist Hospital Research Institute, 6565 Fannin St, MS B5-011 Houston, TX 77030
Email: beoneill@tmhs.org

Abstract: Focused ultrasound systems guided by magnetic resonance imaging (MRI) and thermometry have recently made possible the non-invasive thermal ablation of benign tumors such as uterine fibroids in clinical practice. Much more work is however required in order to make this technology available for the treatment of other forms of cancer. One of the major difficulties is associated with the presence of blood vessels that are an important cause of temperature inhomogeneity preventing the optimal control of temperature required for a successful outcome. To address this problem, focused ultrasound treatments have been simulated for a homogeneous block of muscle-like tissue with either one or multiple discrete vessels. Our results indicate a wide variability in the achieved temperature and thermal dose distributions during the different treatments. We have shown that this variability can be greatly reduced with a treatment planning that takes into account the presence of blood vessels and blood flow.

Keywords: Focused ultrasound, blood vessels, thermal therapy.

1. Introduction

High-intensity ultrasound fields can be focused on targets deep inside the human body into small regions with dimensions on the order of 1 mm. The resulting temperature increase at the focal spot can be used for applications such as cancer cell killing [1,2], to facilitate local drug delivery [3,4], for the control of gene therapy [5] and for blood brain barrier disruption [6]. Focused ultrasound (FUS) systems, which are capable to deliver non-invasive thermal treatments under MRI guidance and using MRI thermometry for temperature measurements, have been recently approved by the Food and Drug Administration for the treatment of uterine fibroids [7]. Although this is a very promising first step, much more work remains to be done to allow the clinical implementation of MRI guided FUS for other medical applications such as thermal ablation of malignant tumors and for enhancing local drug delivery at the cancer location.

The development of an ultrasound treatment planning capable of predicting the complete three-dimensional temperature and thermal dose distributions in the treated area will be essential for the successful clinical implementation of MRI guided FUS.

Besides factors such as absorbed power, thermal conductivity and specific heat, blood flow is the main parameter which determines temperature distribution in tissues. Several models which incorporate the influence of blood flow to some extent have been developed to calculate temperature distribution in tissues. In this study, we will employ the bio-heat transfer model developed by Lagendijk and co-workers [8,9]. This model is capable to describe the thermal behavior of individual vessels and contrary to the more commonly used Pennes bio-heat equation [10], can predict more accurately the overall temperature distribution inhomogeneity.

2. Governing Equations

In our simulations we have used Comsol Heat Transfer module 3.5a with Matlab R2009b. In the vessel domain we have solved the heat transient equation

$$\rho_b c_{pb} \frac{\partial T}{\partial t} + \rho c_{pb} w \frac{\partial T}{\partial z} + \nabla \cdot (k_{blood} \nabla T) = P_{FUS} \quad (1)$$

where T is temperature, ρ_b=1060 kg/m^{3}is the mass density, c_{pb}=*3840* JKg^{-1}K^{-1} is the specific heat, k_{blood}=0.6 W m^{-1} K^{-1} is the thermal conductivity, and w axial is blood velocity by

$$w = 2V_m\left(1 - \frac{r^2}{R^2}\right) \quad (2)$$

with V_m mean blood velocity, R vessel radius and r radial coordinate. The power density distribution P_{FUS} produced by the focused ultrasound field is modeled as in [11]. Plots of the power density distribution through the focus used in the simulations are shown in Fig. 1.

For the vessel sizes and blow flow values, we have employed the data provided by Green for the mesenteric vascular bed of dogs [12].

The incoming blood temperature is assumed to be 37 ^{0}C and the convective flux boundary condition is assumed at the blood vessel exit. A streamline diffusion stabilization factor has been applied in the vessel domain.

In the tissue domain, we have solved the transient heat equation

$$\rho_t c_{pt} \frac{\partial T}{\partial t} + \nabla \cdot \left(k_{eff} \nabla T \right) = P_{FUS} \qquad (3)$$

where c_{pt} = 4000 JKg^{-1}K^{-1} is the specific heat, ρ_t = 1000 kg/m^3 is the mass density and k_{eff} is an effective thermal conductivity which takes into account the blood flow through the smaller vessels surrounding the larger vessels. Its value is assumed to be k_{eff} = 1.8 W m^{-1} K^{-1} [13]. For the tissue domain the boundaries are related to the core temperature by a fixed heat transfer coefficient h simulating a few centimeters of tissue with h=k_{eff}/d and d tissue thickness. The initial temperature for both domains is assumed to be 37 ^{0}C.

3. Numerical results

3.1 Single Vessel and Focused Ultrasound

As a first study, we have examined a single artery with the focus at the vessel center and the vessel running along the axial direction of the transducer. In this case, Eqs. (1-3) can be solved under axial symmetry. For the purpose of illustration, we have assumed the following ultrasound parameters: focus half-power width 4 mm, height 30 mm, peak power density I_0=15 W/ cm^3 (Fig. 1).

We have calculated the temperature increase after one minute insonation for a large artery with radius R=1.5 mm, length L= 200 mm and mean flow velocity V_m= 13 cm s^{-1}; a primary artery with radius R=0.5 mm, length L= 100 mm and mean velocity V_m=8 cm/s; and a secondary

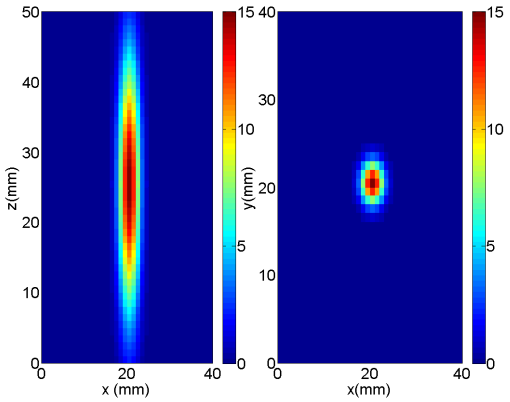

Figure 1. Typical axial and radial power density distributions through the ultrasound focus in W/ cm^3 used in the simulations.

artery with radius R=0.3 mm, L=40 mm and V_m=8 cm/s [12]. The results are shown in Figs. 2, 3, 4. As may be seen, it is very difficult to heat a large artery, while for a smaller artery, such as secondary artery, the temperature increase at the focal plane is significant.

As a second example, we have considered the situation in which the focus is 1 mm from the vessel wall. In such a situation the axial symmetry is lost and a 3D simulation has to be performed. In Fig. 5 we have shown the temperature as a function of time for the focus and a point on the vessel wall at the focal plane. The ultrasound parameters and the vessel parameters are the same as in Fig. 3, i.e. we are considering a primary artery.

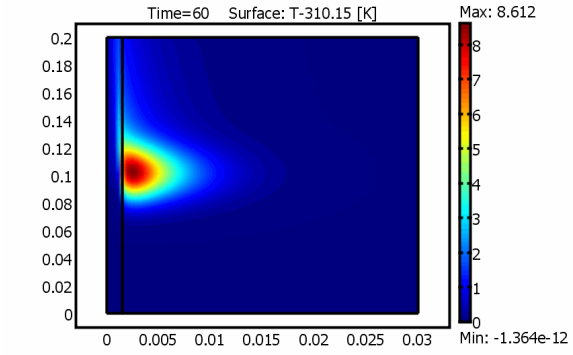

Figure 2. Axial symmetrical temperature increase reached at the end of a 60 s insonation period in a large artery. The spatial units are in meter.

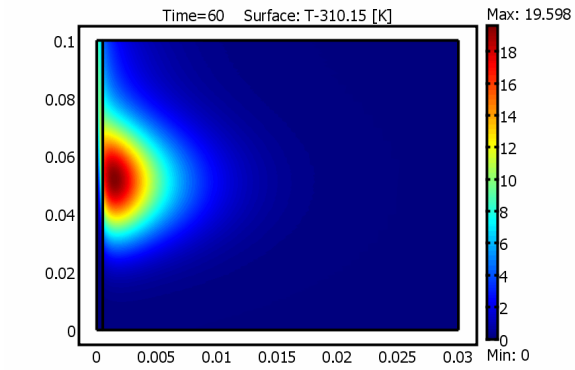

Figure 3. Axial symmetrical temperature increase reached at the end of a 60 s insonation period for a primary artery.

As may be seen, when the ultrasound focus is 1 mm from the vessel wall, conditions of thermal ablation can be very easily reached at the focus but the temperature at the vessel wall is much lower. Hence, blood vessels produce regions of temperature inhomogeneity. For comparison in Fig. 5, we have also shown the temperature reached at the focus when no vessels are present.

3.2 Vessel Pairs and Focused Ultrasound

Up to the level of arterioles, venules and capillaries and with the exception of the superficial venous system, vessels run in counter-flow pairs and therefore it is very important to consider artery-vein vessel pair systems.

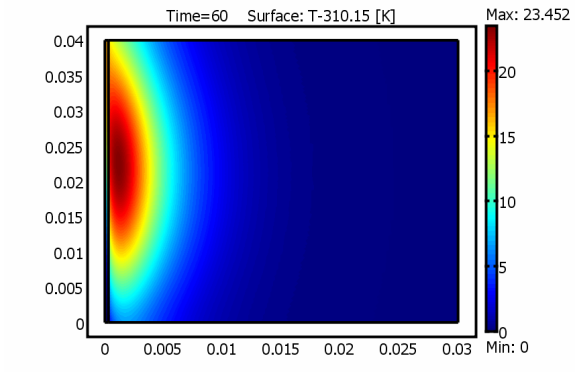

Figure 4. Axial symmetrical temperature increase reached at the end of a 60 s insonation period for a secondary artery.

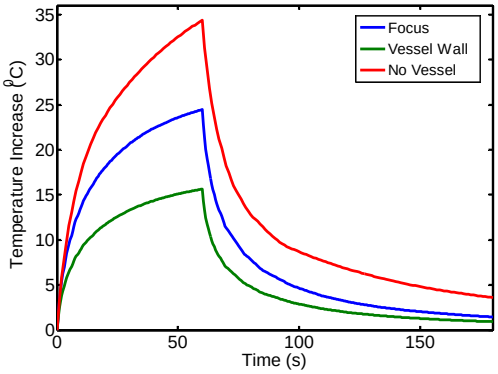

Figure 5. Temperature increase as a function of time for a 60 s insonation period followed by a cooling period of 120 s. The focus is 1 mm from the vessel wall.

With the aim of building complexity incrementally, we have investigated a multiple artery-vein system located in a homogeneous block of muscle-like tissue with dimensions 21 x 21x26 mm^3 (Fig. 6).

For the purpose of illustration, we have considered the vessel pairs to run in parallel along the axial direction of the transducer and having a radius of either 500 μm (3 pairs) or 400 μm (6 pairs). The distance between the artery and vein is 0.8 mm for the 500 μm pair and 0.6 for the 400 μm pair. The focus half-power width and height are assumed to be respectively 3.2 and 24 mm and the power density distribution is varied during the treatment.

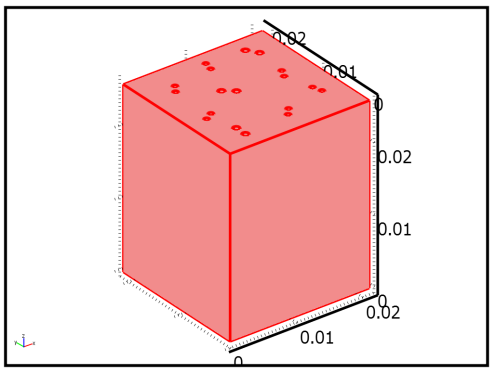

Figure 6. Computational domain consisting of a homogeneous block of muscle-like tissue with dimensions 21 x 21 x 26 mm^3.

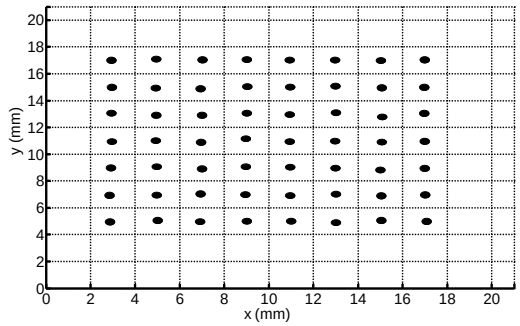

Figure 7. Points in the mid-plane of the computational domain through which the focus is stepped in a random way.

The thermal treatment of the multiple-vessel system is simulated by an ultrasound focus that is stepped through the mid-plane of the computational domain using different delivery methods. In treatment (i): the focus is stepped through the mid-plane of the computational domain in a random way to avoid thermal build-up. In treatment (ii): the focus is stepped along a spiral trajectory starting at the center of the computational domain and going outward. In both cases, the number of insonations is 56 and the duration time for each insonation is 20 s followed by a 5 s cooling period for a total insonation time of 1395 s, about 23 minutes.

Fig. 7 shows the points through which the focus is stepped for treatment (i). The points are separated by a distance of 2 mm. The focus is stepped in a random way though the 56 points with the condition that the distance between one insonation and the next is at least 8 mm.

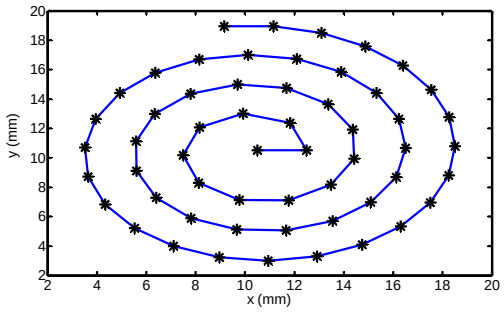

Figure 8. Points in the mid-plane of the computational domain through which the focus is stepped following a spiral trajectory.

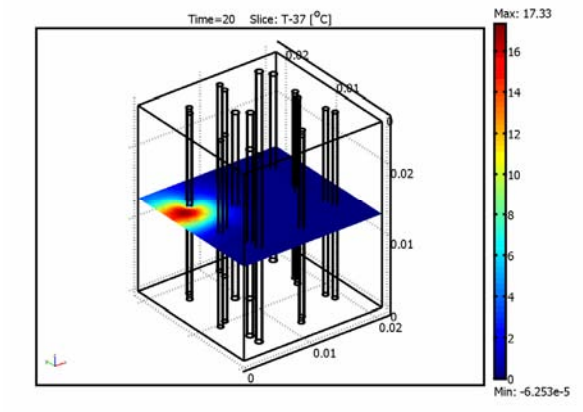

Figure 9. Temperature distribution reached in the mid-plane at the end of the first insonation period for the random insonation treatment with peak power density of 17.5 W/cm^3.

In the spiral trajectory treatment, illustrated in Fig. 8, the distance between two successive turns is 2 mm and the distance between two successive insonation points is also 2 mm.

Fig. 9 shows as an example of temperature distribution in the mid-plane at the end of the first insonation period (20 s) for treatment (i). The peak power density the simulations is 17.5 W/cm^3.

3.3 Thermal Dose Calculation

The overall performance of the treatments is evaluated by calculating the thermal dose for the mid-plane of the computational domain. We have employed the following thermal dose definition [14]

$$TD(t) = \int_0^t \mathcal{R}^{43-T(t')} dt' \qquad (4)$$

with $\mathcal{R}$

$$\mathcal{R} = \begin{cases} 0.25 & T(t) < 43\,^0C \\ 0.5 & T(t) \geq 43\,^0C \end{cases} \qquad (5)$$

At 43 ^{0}C, a treatment duration of 240 min has been introduced as a reference for thermal lesion formation [15]. All thermal dose calculations are normalized to this standard, with a thermal dose

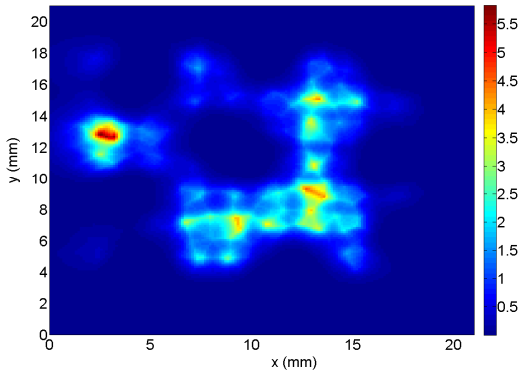

Figure 10. Total thermal dose accumulation in the mid-plane for the random insonation treatment with fixed power.

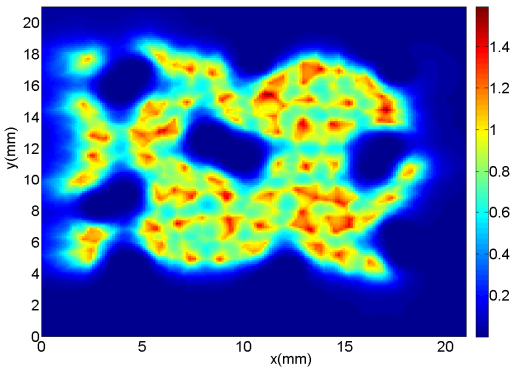

Figure 12. Total thermal dose accumulation in the mid-plane for the random insonation treatment with variable power**.**

of one corresponding to the condition that will lead to protein denaturation and tissue necrosis. At first, we have calculated the thermal dose in the mid-plane for treatments (i) and (ii) while keeping the power density distribution fixed during the treatment with I_0=17.5 W/cm^3.The results of the simulations are shown in Figs. 10 and 11. As may be seen in the plots, when the power is kept fixed, the thermal dose deposition varies greatly, with the highest peak thermal dose deposition observed for the spiral treatment. In both treatments, underdosage around the vessel pairs is clearly visible.

We have then changed the power distribution so that the peak thermal dose deposition remains in the range between 230 to 250 min for each insonation. The total thermal dose at the mid-plane of the computational domain for both treatments is shown in Figs. 12 and 13. Therefore, when the power is changed during the treatments, the thermal dose deposition is similar in both cases and the delivery method does not appear to be as important as in the previous example. Furthermore, the thermal dose is more uniformly distributed. However, underdosage is still visible around the vessel pairs.

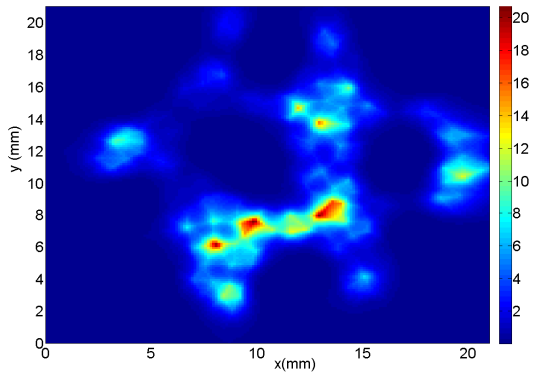

Figure 11. Total thermal dose accumulation in the mid-plane for the spiral insonation treatment with fixed power.

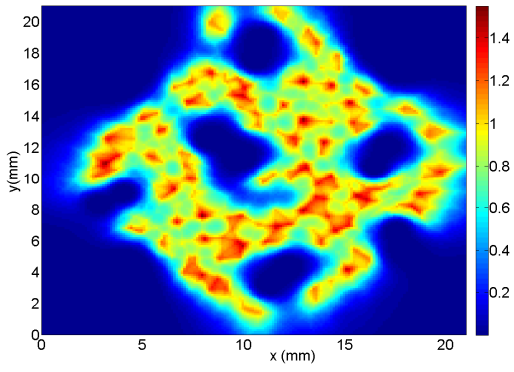

Figure 13. Total thermal dose accumulation in the mid-plane for the spiral insonation treatment with variable power**.**

4. Discussion

Blood flow strongly affects the temperature distribution during an ultrasound thermal treatment.

When the treatments are delivered without taking into account the cooling effect exerted by the blood flow, the resulting thermal dose is highly variable with regions of thermal damage, regions of underdosage close to the vessels, and areas in between these two extremes. This is true for both delivery methods examined in this investigation. However, the random insonation treatment with fixed power has a much lower peak thermal dose, about 3 to 4 times smaller than the peak thermal dose obtained with the spiral delivery method.

When the power has been adjusted as to have a thermal dose accumulation at each insonation close to the threshold for thermal damage, the resulting total thermal dose distribution is more uniformly distributed in both cases. Nevertheless, areas of thermal damage and underdosage are still present.

Since the power required to keep the thermal dose close to the threshold for thermal damage varies greatly from one insonation to next even for nearby points, only a treatment planning able to predict the overall temperature distribution as a function of acoustic energy absorption, blood vessel position and blood flow would be able to produce the required thermal dose distribution. Such a treatment planning however would require the exact perfusion and the location of the thermally significant intermediate blood vessels (0.3-0.8 mm) of each individual patient. Such information is currently not available with the required resolution. To compensate for this missing information, thermal control strategies based on MRI thermometry could be implemented. These strategies will greatly benefit from an improvement in the current resolution of MRI thermometry which is of the order of one mm while temperature heterogeneity is expected to be present up to a level of about 0.3 mm.

5. Conclusions

FUS has been proposed for a variety of therapeutic applications such as tumor thermal ablation and as a way to increase local drug delivery for cancer treatment. The results obtained in preclinical studies are encouraging but a better control of the temperature distribution together with the knowledge of which level of temperature homogeneity is necessary in order to achieve a successful outcome is required.

Although our investigation is only preliminary and does not take into account the complexity of the real anatomy, it suggests the importance of a treatment planning that takes into account the presence of blood vessels and blood flow. In addition, it seems to indicate that the overall temperature heterogeneity caused by blood flow could be greatly improved during a FUS treatment provided the availability of blood vessel data and an efficient tailored strategy for delivering the ultrasound treatment.

6. References

1. C J Diederich, Thermal ablation and high-temperature thermal therapy: Overview of technology and clinical implementation, *Int J Hypertheria*, **21,** 745-53 (2005)
2. K Hynynen, MRI-guided focused ultrasound treatments, *Ultrasonics*, **50,** 221-9 (2010)
3. B E O'Neill, C Karmonik, E Sassaroli, and K C P Li 2009, Translational studies of pulsed HIFU enhanced tissue permeability: mechanisms in mice and rabbit models, *IEEE International Ultrasonics Symposium*, Rome (Italy), September 20-23, (2009)
4. B E O'Neill, H Vo, M Angstadt, K C P Li, T P Quinn, V Frenkel, Pulsed High Intensity Focused Ultrasound Mediated Nanoparticle Delivery: Mechanisms and Efficacy in Murine Muscle, *Ultrasound Med. Biol.,* **35**, 416-24 (2008)
5. R Deckers, B Quesson, J Arsaut, S Eimer, F Couillaud and C T W Moonen, Image-guided, noninvasive, spatio-temporal control of gene expression, *PNAS*, **106**, 1175-80 (2009)
6. N McDannold, N Vykhodtseva, F A Jolesz, K Hynynen, MRI Investigation of the Threshold for Thermally Induced Blood–Brain Barrier Disruption and Brain Tissue Damage in the Rabbit Brain, *Magn. Reson. Med.,* **51,** 913–23 (2004)
7. E A Stewart, B Gostout, J Rabinovici, H S Kim, L Regan and C M Tempany, Sustained relief of leiomyoma symptoms by using focused ultrasound surgery, *Obstet. Gynecol.,* **110**, 279–87 (2007)

8. A N T J Kotte, G M J van Leeuwen, J de Bree, J F van der Koijk, J Crezee and J J W Lagendijk, A description of discrete vessel segments in thermal modeling of tissues, *Phys. Med. Biol.*, **41**, 865–84 (1996)
9. A N T J Kotte, G M J van Leeuwe and J J W Lagendijk, Modeling the thermal impact of a discrete vessel tree, *Phys. Med. Biol.*, **44**, 57–74 (1999)
10. H Pennes, Analysis of tissue and arterial blood temperatures in the resting human forearm, *J. Appl. Phys.*, **1**, 193-22 (1948)
11. J Palussiere, R Salomir, B Le Bail, R Fawaz, B Quesson, N Grenier, and C. T.W. Moonen, Feasibility of MR-Guided Focused Ultrasound With Real-Time Temperature Mapping and Continuous Sonication for Ablation of VX2 Carcinoma in Rabbit Thigh, *Magn. Reson. Med.*, **43**, 342–7 (2000)
12. H D Green, Circulatory System: Physical Principles, *Medical Physics* vol II, Ed O Glassee, pp 228-51, Medical Year Book Publishers, Chicago (1950)
13. J Creeze and J J W Lagendijk, Experimental verification of bioheat transfer theories: measurement of temperature profiles around large artificial vessels in perfused tissue, *Phys. Med. Biol.*, **35**, 905-23(1990)
14. S A Sapareto and W C Dewey, Thermal dose determination in cancer therapy, *Int. J. Radiat. Oncol. Biol. Phys.*, **10**, 787–800 (1984)
15. C A Damianou, K Hynynen and X B Fan, Evaluation of accuracy of a theoreticalmodel for predicting the necrosed tissue volume during focused ultrasound surgery, *IEEE Trans. Ultrason. Ferroelectr. Freq. Control*, **42**, 182–7 (1995)

7. Acknowledgements

Work supported by NIH grant # 5-R01-EB009009-01.